# Flow-induced polymer translocation through narrow and patterned channels

Arash Nikoubashman[1,a)] and Christos N. Likos[2,b)]
[1]*Institute of Theoretical Physics, Heinrich Heine University of Düsseldorf, Universitätsstraße 1, D-40225 Düsseldorf, Germany*
[2]*Faculty of Physics, University of Vienna, Boltzmanngasse 5, A-1090 Vienna, Austria*

(Received 26 April 2010; accepted 25 June 2010; published online 16 August 2010)

We consider linear and branched polymers driven through narrow and patterned channels by imposing a Poiseuille flow on the ambient solvent. We establish, by means of scaling arguments, that the translocation probability of dendrimers through the pore is independent of the number of monomers and that it takes place above a viscosity-dependent critical external current. When the channel walls are smooth, the translocation times of linear and branched polymers with the same monomer number are very similar. However, for walls that are decorated with attractive patches, dramatic differences show up: whereas a dendrimer successively docks at the patches and "walks" from one to the next, being carried away by the solvent flow, linear chains spread themselves along the channel wall without achieving translocation within simulation times. Our findings are relevant for, e.g., drug delivery through dendritic carrier molecules in capillary arterioles. © *2010 American Institute of Physics*. [doi:10.1063/1.3466918]

## I. INTRODUCTION

Translocation of polymers through narrow holes, which allow for the passage of one monomer at a time and exclude the formation of hairpins, is a problem of high relevance in biology and industry, posing at the same time a challenge for theory and simulations. Accordingly, a great deal of experimental, theoretical, and simulational effort has been devoted to it, and we refer to Ref. 1 for a list of relevant references. In most cases, a flat membrane with a single opening is considered, with a linear chain of $N$ monomers translocating from one side of it to the other. The driving forces behind this phenomenon can have a multitude of physical origins, including a chemical potential gradient across the partition,[2–4] external fields, such as voltage,[5] or preferential adsorption of the chain on one side of the membrane.[1,6] Di Marzio and Mandell showed,[7] within the framework of a simplified model, that a first-order translocation phase transition occurs for chains when $N\to\infty$. An issue that has been discussed at great lengths within the context of translocation is the scaling of the passage time through the hole and its dependence on $N$ and the external fields imposed on the setup. Different theories and approaches have been put forward. Computer simulations by Milchev *et al.*[1] confirm the prediction of Chuang *et al.*[8] that the translocation dynamics of self-avoiding chains is anomalous, with the passage time scaling as $\sim N^{2\nu+1}$ ($\nu\cong 0.59$ is the Flory exponent for self-avoiding chains) below the adsorption threshold and as $\sim N^{1.65}$ above it. The case of unbiased translocation has also been recently studied by simulation.[9]

A closely related problem is the escape of a polymer chain through a long channel, for which the driving force can be either a chemical potential imbalance[4,5] or, as in the present work, solvent flow. Indeed, the flow behavior of macromolecules through narrow channels has recently attracted considerable attention due to its relevance concerning, for example, biological applications of microfluidics,[10] sequencing DNA by passing it through nanopores,[11,12] and the passage of biomolecules through membrane channels.[13] Here, the issue of interest is whether the external current $J$ is strong enough to cause insertion, and then suction, of the polymer inside the narrow channel. Both for linear and for randomly branched polymers, de Gennes *et al.*[14] have established that the critical suction current is independent of the degree of polymerization, correcting thereby the originally wrong prediction of $N$-dependence for the latter.[15]

The process by which a polymer moves through a narrow channel can be divided into three stages. First of all, the polymer must find the opening, second it must squeeze into the constriction, and only then can it move through the microchannel. In this work, we focus on the latter two steps for the case of *dendrimers*, which are regularly branched polymers, in contrast to the aforementioned randomly branched objects. Our approach is similar to the recent work of Markesteijn *et al.*,[16] but we focus on dendritic instead of linear polymers and we consider different aspects of the problem, focusing on translocation times and wall patterning; further, our simulation technique is a different one from that in Ref. 16 above. This subject has not only theoretical interest, but it is relevant to applications as well since dendrimers are used as drug carrier molecules, which have to travel downstream along arteries or capillary-sized arterioles driven by the bloodstream. We put forward a theoretical approach to predict that the critical current for narrow channel openings is independent of $N$ also for low-generation dendrimers, while, evidently, it vanishes for channels whose

a)Electronic mail: arash.nikoubashman@uni-duesseldorf.de.
b)Electronic mail: christos.likos@univie.ac.at.

 

width exceeds the molecular size. We further perform hybrid simulations that couple hydrodynamic flow with molecular motion to analyze the dependence of passage times on the width and patterning of the channel walls, finding that the molecule "docks" on attractive patches on the wall and has finite residence times there until it is further carried away by the incipient solvent flow. A comparison between dendrimers and linear chains of the same molecular weight reveals no significant differences between the two for the case of smooth walls but yields drastically different behavior for patterned ones.

The rest of this work is organized as follows. First, in Sec. II, we derive an analytic expression for the threshold flux needed to push a dendrimer into a narrowing. Then, we describe the employed polymer model in Sec. III A and introduce our simulation method briefly in Sec. III B. The results are then presented and discussed in Sec. IV. Finally, we summarize the findings and draw our conclusions in Sec. V.

## II. THEORY OF INJECTION THRESHOLDS

This work is mainly concerned with injection of dendrimers in narrow channels, whereby we will be making systematic comparisons with *linear* polymers as well, to establish the salient similarities and differences between the two. The lateral opening (width $D$) of the channel will be thereby of the order of the dendrimer size, the latter being typically quantified via the radius of gyration $R_G$. Whereas for widths considerably larger than the dendrimer size, its transport through the channel is guaranteed, the same is not true if $D<R_G$. Here, we anticipate the existence of a threshold for the current, below which no translocation takes place. In the following, we estimate this value and we establish that it is independent of the dendrimer's degree of polymerization. We limit ourselves to low-generation dendrimers ($G=2-4$), which can be described as "compact objects."

We commence with a short summary of known results about the flow injection of fractal and deformable objects, such as polymers, into narrow channels. A flexible linear polymer in a dilute solution enters a pore of diameter $D<R_G$ only when it is pushed into the narrowing by a solvent flux $J$ that exceeds a certain threshold value $J_c$. Here, the flux $J$ is the total current, defined as the volume of solvent passing through a cross-section of the channel in the unit of time. The value of the threshold flux, $J_c$, has been derived in Ref. 15 by using Flory-type scaling arguments, based on the blob model for polymers,[17] with the result

$$J_c \simeq \frac{k_B T}{\eta}, \tag{1}$$

where $k_B$ is the Boltzmann's constant, $T$ is the absolute temperature, and $\eta$ is the dynamic viscosity of the solvent. This finding is quite surprising since it is completely *independent* of the number of monomers $N$ and the internal polymer structure.

In the following, we employ a similar approach in order to determine the injection threshold in the case of regularly branched polymers, i.e., dendrimers, where, because of their peculiar architecture and the ways their monomers order, no simple blob model is applicable. A simulation snapshot of a dendrimer is shown in Fig. 1. In particular, it has been found by extensive simulations[18] that for low-generation dendrimers, $G=2-4$, the size $R_G$ scales with the number of monomers $N$ as $R_G \sim N^{1/3}$. This is reminiscent of a compact object akin, e.g., to linear chains in a poor solvent, but the situation is more subtle because low-generation dendrimers are nevertheless soft and deformable.[19–21] At the same time, since there are clear steric limitations in an object for which the number of monomers grows exponentially with the generation number, there is no formal $N\to\infty$-limit for dendrimers, at least not for a spacer length of unity between successive generations. As a result, the gyration radius of low-generation dendrimers is of the same order as the monomer length; see, e.g., Table I of this work and Ref. 18.

TABLE I. The radii of gyration for linear and dendritic polymers.

| Polymer architecture | $N$ | $R_G$ |
|---|---|---|
| Linear | 32 | $3.85\pm0.65$ |
| Linear | 62 | $5.63\pm0.94$ |
| Linear | 92 | $7.19\pm1.24$ |
| Dendritic (G2) | 14 | $1.62\pm0.03$ |
| Dendritic (G3) | 30 | $2.18\pm0.04$ |
| Dendritic (G4) | 62 | $2.78\pm0.04$ |

We aim at employing a Flory-type theory for dendrimers under flow, akin to that put forward in Ref. 14 for randomly branched polymers, and which modified the original, slightly flawed arguments presented in Refs. 15 and 22. The first task thereby is to formulate the form of the theory for dendrimers *in the bulk*. Here, the problem already arises that if one follows the standard way and writes down an elastic term of the form $\sim k_B T R^2/R_0^2$, $R_0 \sim \ln N$ being the ideal dendrimer size, the aforementioned correct scaling $R_G \sim N^{1/3}$ for low-generation dendrimers does *not* come out. Therefore, we follow a heuristic modification. Instead of using the ideal dendrimer size, $R_0$, in the denominator of the elastic contribution, we introduce an arbitrary length scale $R_x$, which scales as $R_x \sim N^x$, with an as of yet undetermined exponent $x$. Accordingly, we write a Flory-type reduced free energy as the sum of the elastic and excluded-volume terms as

$$\beta F_{\mathrm{Fl}}(R) = \frac{NR^2}{R_x^2} + \frac{N^2 a^3}{R^3}, \tag{2}$$

with $\beta=(k_B T)^{-1}$ and $a$ denoting the monomer size. Notice the additional factor $N$ in the elastic energy, which arises from the peculiar dendritic architecture and reflects the fact that a typical number of $N$ chains are deformed when a dendrimer has linear size $R$. This $N$-factor plays a role analogous to the functionality $f$ of $f$-armed star polymers. Minimization with respect to $R$ yields $R_G \sim N^{(1+2x)/5}$ and *requiring* that this reproduces the correct simulation result,[18] $R_G \sim N^{1/3}$, yields $x=1/3$. Alternatively, one could have argued that the first and second terms on the right-hand side must have the same $N$-exponent when $R \sim N^{1/3}$, namely, they must be a linear function of the degree of polymerization.

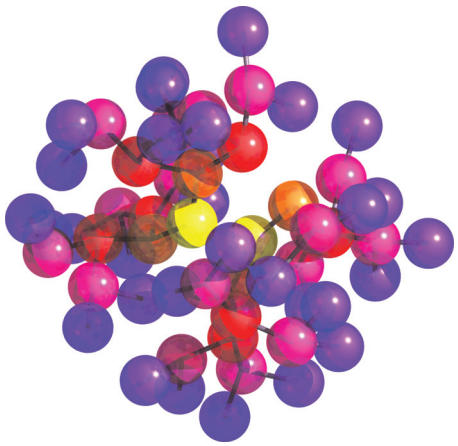

FIG. 1. Simulation snapshot of a G4-dendrimer.

We now turn to the situation in which a dendrimer is pushed by a current $J$ in front of the opening of a narrow channel of width $D$, schematically depicted in Fig. 2. Note that since dendrimers are small objects, a hierarchy of length scales $a \ll D \ll R_G$ is not possible, and we rather have $a \sim D < R_G$. However, we will keep the discussion general in what follows and maintain both length scales, $a$ and $D$, as independent parameters in the scaling argument to follow. Under the conditions depicted in Fig. 2, it can happen that the dendrimer only partially penetrates the channel, having a penetration length $y$ and $P < N$ of its monomers inside. Similar to the approach in Ref. 14, we first estimate the dependence of $y$ on $P$ by writing down an expression for the free energy of the confined part in analogy with Eq. (2), i.e.,

$$\beta F(y) = \frac{y^2}{R_x^2(P)} + \frac{P^2 a^3}{yD^2}, \tag{3}$$

where $R_x(P) \sim P^{1/3}$. In comparing Eq. (3) with Eq. (2), note the absence of an additional factor $P$ in the elastic energy of the former since we anticipate that only a few monomers are confined in the partially injected state and thus there is no reason to believe that $P$ chains are compressed. Minimizing Eq. (3) with respect to $y$, we obtain the scaling relation

$$\frac{y}{D} \simeq \left(\frac{a}{D}\right)^{5/3} P^{8/9}. \tag{4}$$

The specific volume $\xi^3(y)$ available to each of the $P$ confined monomers is given by the space-filling condition,

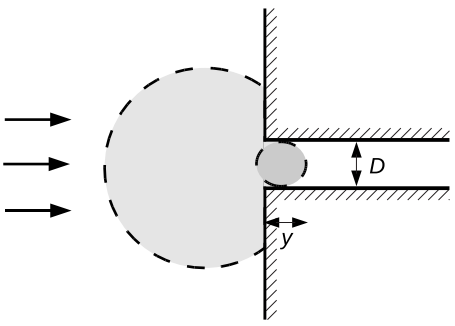


FIG. 2. A partly injected dendrimer inside a narrow channel with width $D$.

$$\frac{a^3}{\xi^3(y)} = \frac{Pa^3}{yD^2}. \tag{5}$$

Using Eqs. (4) and (5), we readily obtain

$$\xi(y) = y^{1/3} D^{2/3} P^{-1/3} = a \left(\frac{D}{a}\right)^{3/8} \left(\frac{D}{y}\right)^{1/24}. \tag{6}$$

It follows that $\xi(y)$ has a slow decrease as $y$ grows.

Within the confined part, there evidently exist $yD^2/\xi^3(y)$ monomer blobs, each of which can be assigned a free energy cost $k_B T$. Counteracting to it, there is a hydrodynamic contribution from the drag of the flowing solvent, resulting in the total free energy $\mathcal{F}(y)$ that has the form

$$\mathcal{F}(y) = \mathcal{F}_{\text{conf}}(y) + \mathcal{F}_{\text{hyd}}(y) = k_B T \frac{yD^2}{\xi^3(y)} - \int_0^y f_{\text{hyd}}(y')dy', \tag{7}$$

with the hydrodynamic force $f_{\text{hyd}}$ being expressed as a Stokes drag per monomer, yielding

$$f_{\text{hyd}}(y) \simeq \eta \xi(y) v(D) \frac{yD^2}{\xi^3(y)}, \tag{8}$$

where $v(D) = J/(\pi D^2)$ is the local solvent velocity. Introducing expression (6) above and carrying out the algebra, we obtain the scaling laws,

$$\mathcal{F}_{\text{conf}}(y) \cong k_B T a^{-15/8} D^{3/4} y^{9/8} \tag{9}$$

and

$$\mathcal{F}_{\text{hyd}}(y) \cong -\eta J a^{-5/4} D^{-5/6} y^{25/12}. \tag{10}$$

Evidently, the sum of Eqs. (9) and (10), seen as a function of the confinement length $y$, initially grows with $y$ since $\mathcal{F}_{\text{conf}}$ dominates for small $y$-values and eventually drops because $\mathcal{F}_{\text{hyd}}$ takes over for large $y$ values. The total curve has a maximum at the position $y^*$, and the value $\mathcal{F}(y^*)$ corresponds thereby to a "suction free energy barrier" that must be overcome before the whole of the molecule is inserted into the channel. From Eqs. (9) and (10), the value $y^*$ is easily calculated as

$$y^* \cong \left(\frac{k_B T}{\eta J}\right)^{24/23} D \left(\frac{D}{a}\right)^{15/23}. \tag{11}$$

The resulting free energy barrier height reads as

$$\beta \mathcal{F}(y^*) \cong \left(\frac{k_B T}{\eta J}\right)^{27/23} \left(\frac{D}{a}\right)^{60/23}. \tag{12}$$

Suction occurs when the barrier height is of the order of the thermal energy $k_B T$; thus setting $\beta \mathcal{F}(y^*) \cong 1$ in Eq. (12) above, we obtain the critical suction current $J_c$ as

$$J_c \cong \frac{k_B T}{\eta} \left(\frac{D}{a}\right)^{20/9} \cong \frac{k_B T}{\eta}, \tag{13}$$

the last equality following from the aforementioned fact that $D \cong a$. Thus, similar to linear and randomly branched polymers, we find that also for dendrimers the critical current is independent of the degree of polymerization, a result that has been confirmed in our simulations (see Sec. IV below). How-

ever, in contrast to those two other polymer classes, the penetration length $y^*$ at $J=J_c$ is of the order of $a$, and, according to Eq. (4), the number of sucked monomers there is of the order of unity. Due to the dendrimer architecture, a state in which a subcritical current causes a significant part of the molecule to be within the channel, whereas the rest remains outside, is not feasible for dendrimers: the suction of a few monomers is sufficient to deform the whole molecule accordingly and to bring about injection of the same in the channel.

The small value of the critical penetration length $y^*$ is a peculiarity of the dendritic architecture and the compact character of the molecule. Indeed, squeezing a few (terminal) monomers of the dendrimers within the channel has the effect of "flattening" a part of the dendrimer lying outside the channel as well, so that most of the molecule is already deformed and can be pushed into the channel. The same property lies in the heart of the apparent paradox that $J_c$ grows with $D$ [see Eq. (13) above]. To understand this, it must be noted that, according to Eq. (11), the critical penetration length $y^*$ grows with $D$ as well so that the *same* penetration for a *wider* channel causes less deformation of the molecule and thus its shape is not suited to suction. A *stronger* current is thus needed to push part of the molecule in the channel and cause significant deformation to the remaining part outside the channel so that the latter can get squeezed into the pore as well. However, these findings are only valid for low-generation dendrimers with spacer lengths $P=1$. For dendrimers with high $G$ and/or $P$ values, we do not expect these arguments to hold anymore, and it is possible that $J_c$ will then depend on details of the molecular architecture.

## III. SIMULATION

### A. Polymer model

A common approach for physically modeling the configuration of polymers is to treat the individual monomers (Kuhn segments) as spherical beads interacting by potentials that depend on their mutual separation. Accordingly, we consider two different types of pair interactions between the individual monomers. The first contribution is a short-ranged, purely repulsive interaction given by a simple, shifted, and truncated Lennard-Jones potential, which models the short-range, excluded-volume interactions between the monomers,

$$U_{\mathrm{mm}}(r)=\begin{cases}4\epsilon\left[\left(\frac{\sigma}{r}\right)^{12}-\left(\frac{\sigma}{r}\right)^{6}\right]+\epsilon, & r\le r_{\mathrm{cut}}\\ 0, & r>r_{\mathrm{cut}},\end{cases} \tag{14}$$

with $r=|\mathbf{r}_i-\mathbf{r}_j|$ denoting the separation between the monomers $i$ and $j$, whose position vectors are $\mathbf{r}_i$ and $\mathbf{r}_j$, respectively. Equation (14) introduces an energy scale $\epsilon$ and a length scale $\sigma$, which will be taken as the units of energy and length in what follows. Note that $\sigma$ is the same as $a$, the monomer size introduced in Sec. II above. The cutoff distance in Eq. (14) above has been chosen as $r_{\mathrm{cut}}=2^{1/6}\sigma$, rendering the monomer-monomer interaction purely repulsive and thus suitable for an effective description of athermal solvents. Boltzmann's constant $k_B$ is set to unity as well, and we choose for the temperature $T=\epsilon=1$.

To model the chemical links, bonded monomers interact via a finite extendible nonlinear elastic (FENE) potential $U_{\mathrm{FENE}}(r)$, which is given by[23]

$$U_{\mathrm{FENE}}(r)=\begin{cases}-U_0\left(\frac{r_0}{\sigma}\right)^2\ln\left[1-\left(\frac{r}{r_0}\right)^2\right], & r\le r_0\\ \infty, & r>r_0,\end{cases} \tag{15}$$

where the location of divergence $r_0$ determines the maximum bond length between two monomers and can be used along with $U_0$ to tune the stiffness of the polymer. In our simulations, we have chosen $U_0=5.0$ and $r_0=4.0$, leading to rather soft and elastic connections. This is the same model used for dendrimers under shear in Ref. 24. Although the choice of $r_0=4.0$ makes bond crossing technically possible, such unphysical moves hardly take place: at subcritical currents, the amount of sucked monomers is very small and only terminal; at supercritical currents, the dendrimer is "carried along" with the current, and internal fluctuations are essentially decoupled from the transport process since the current acts on dragging individual monomers. Effects on docking should also be essentially irrelevant because it is the outer generations that dock, and these make a "walk" along the walls, which does not involve crossing of bonds.

In addition to these intramolecular forces, the polymer interacts with the system boundaries (i.e., the channel walls) via the potential $U_{\mathrm{wall}}$, which is given by

$$U_{\mathrm{wall}}(x)=\begin{cases}\frac{2}{3}\pi\epsilon\left[\frac{2}{15}\left(\frac{\sigma}{x}\right)^9-\left(\frac{\sigma}{x}\right)^3+(1-\lambda_{\mathrm{w}})\frac{\sqrt{10}}{3}\right], & 0\le x\le(2/5)^{1/6}\sigma\\ \frac{2}{3}\pi\epsilon\lambda_{\mathrm{w}}\left[\frac{2}{15}\left(\frac{\sigma}{x}\right)^9-\left(\frac{\sigma}{x}\right)^3\right], & x>(2/5)^{1/6}\sigma,\end{cases} \tag{16}$$

for a wall lying parallel to the $(y,z)$-plane at $x=0$. The total external potential caused by both walls separated by $D$ is thus given by $U_{\mathrm{ext}}(x)=U_{\mathrm{wall}}(x)+U_{\mathrm{wall}}(D-x)$. The attractiveness of the potential can be adjusted by the parameter $\lambda_{\mathrm{w}}$. In Fig. 3, we show plots for the extreme cases $\lambda_{\mathrm{w}}=0.0$ (purely repulsive) and $\lambda_{\mathrm{w}}=1.0$ (attractive wall) for a slitlike channel

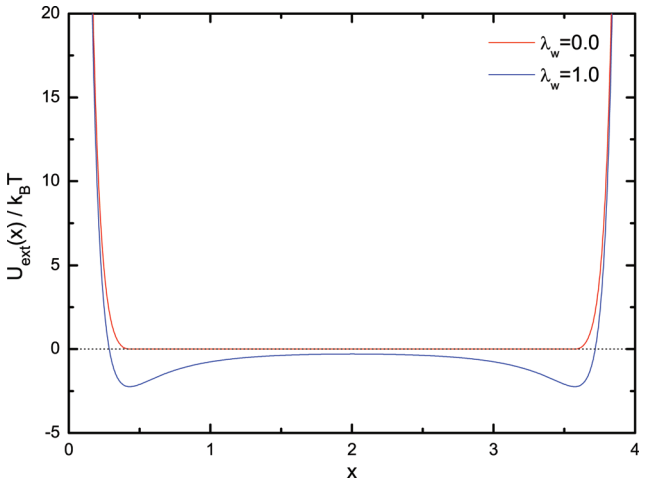


FIG. 3. The external wall potential acting on a monomer for a channel with width $D=4.0$; see Eq. (16). The choice $\lambda_w=0.0$ mimics purely repulsive walls, while $\lambda_w=1.0$ adds a long-ranged attractive tail to the potential.

of width $D=4.0$.

The linear polymers are then created by a three-dimensional self-avoiding random walk. For dendrimers, we use the same approach but start with a central pair of joined monomers, the so-called zeroth generation $G=0$. A successive layer of monomers is then formed by connecting two additional beads to each outer monomer of generation $G$. Thus, the functionality of the dendritic structure is $f=3$, and the number of monomers $N(G)$ taking part to a given generation $G$ follows a simple power law, i.e., $N(G)=2^{G+1}$.

The analysis of the shape and size of isolated dendrimers plays a key role in understanding not only the properties of the molecules themselves but also the thermodynamics of concentrated dendrimer solutions in a coarse-grained approach.[25] A convenient measure for the *overall size* of polymers is given by the so-called *radius of gyration* $R_G$, defined as

$$R_G^2 = \frac{1}{N}\left\langle \sum_{i=1}^{N} (\mathbf{r}_i - \mathbf{r}_c)^2 \right\rangle, \tag{17}$$

where $\mathbf{r}_c$ denotes the center of mass position and $\langle \cdots \rangle$ denotes the statistical average over all conformations. In order to quantify the structural properties and the alignment of polymers in flow, we consider the average gyration tensor of the molecule, $G_{\alpha\beta}$, defined as

$$G_{\alpha\beta} = \frac{1}{N}\sum_{i=1}^{N} \langle r_{i,\alpha} r_{i,\beta} \rangle, \tag{18}$$

where $r_{i,\alpha}$ is the $\alpha$-component of the position vector of the $i$th monomer relative to the center of mass and $\alpha,\beta \in \{x,y,z\}$ denote Cartesian coordinates. This quantity is called the average gyration tensor $G_{\alpha\beta}$ and is directly accessible in scattering experiments. Furthermore, it is obvious that its diagonal components, $G_{\alpha\alpha}$, are the squared radii of gyration in $\alpha$ direction. The bulk values of the gyration radii for the systems simulated in this work are summarized in Table I.

### B. Simulation method

In this work, we model the hydrodynamic interactions mediated by the solvent as faithfully as computationally feasible by employing a hybrid simulation approach, in which standard molecular dynamics (MD) algorithms for the polymer are combined with the multi-particle-collision dynamics (MPCD) simulation technique.[26,27] MPCD is a mesoscopic, particle-based method consisting of alternating *streaming* and *collision* steps and offers an alternative to Lattice–Boltzmann approach. The latter has been employed in the recent work of Markesteijn *et al.*,[16] which deals with injection of linear chains into nanopores.

In MPCD, solvent particles are noninteracting, but they undergo stochastic collisions among themselves and the dissolved monomers according to well-defined rules. During the streaming step, the solvent particles propagate ballistically so that the position of a solvent particle $i$ at the next time step $t+\Delta t$ is given by

$$\mathbf{r}_i'(t+\Delta t) = \mathbf{r}_i'(t) + \Delta t \mathbf{v}_i'(t), \tag{19}$$

where $\mathbf{r}_i'(t)$ denotes the position and $\mathbf{v}_i'(t)$ denotes the velocity of the $i$th solvent particle at time $t$. In the collision step, the $N_s$ solvent particles are first sorted into $N_{\text{cells}}=N_x\times N_y\times N_z$ cubic cells $\mathcal{V}_j$ of edge length $a=\sigma$. Then, their velocities $\mathbf{v}_i'$ are transformed via

$$\mathbf{v}_i'(t+\Delta t) = \mathbf{u}_j(t) + \Omega(\alpha)[\mathbf{v}_i'(t) - \mathbf{u}_j(t)], \tag{20}$$

with the center of mass velocity $\mathbf{u}_j$ of the corresponding cell and the norm-conserving rotation matrix $\Omega$ around a fixed angle $\alpha$. The mean free path of a solvent particle is hence given by $\lambda=\Delta t\sqrt{T}$, and it has been shown in Ref. 28 that Galilean invariance is violated for $\lambda < a/2$. With the purpose of avoiding such a nonphysical behavior, all lattice cells $\mathcal{V}_j$ are shifted by a randomly chosen vector drawn from the interval $[-\mathbf{a}/2,+\mathbf{a}/2]$ before each collision step.

Whereas the above-described rules governing MPCD solvent dynamics are general, the simulation of specific flow patterns for the solvent requires special care. In Ref. 24, the rules to generate steady shear with shear rate $\dot{\gamma}$ have been laid out; here, we are interested in flow generated by a constant pressure gradient along the channel. Such a flow is driven by the pressure gradient parallel to the flow direction and is slowed down by viscous drag along both plates so that these forces are in balance. A fluid stream of this kind through a pipe of uniform cross-section is known as Hagen–Poiseuille flow, and it has been simulated according to the rules set out in what follows.

Several methods exist for creating such a flow, for instance, forced, gravitational, and surface-induced approaches. The forced flow has been considered in Refs. 26, 29, and 30, where the pressure gradient is mimicked by hanging a virtual pump to the inlet of the channel. However, it has been shown in Ref. 31 that this approach has several drawbacks. First of all, a considerable deformation of the velocity-field and density profiles can occur at the inlet and outlet of the channel. In addition, a gradual density drop of

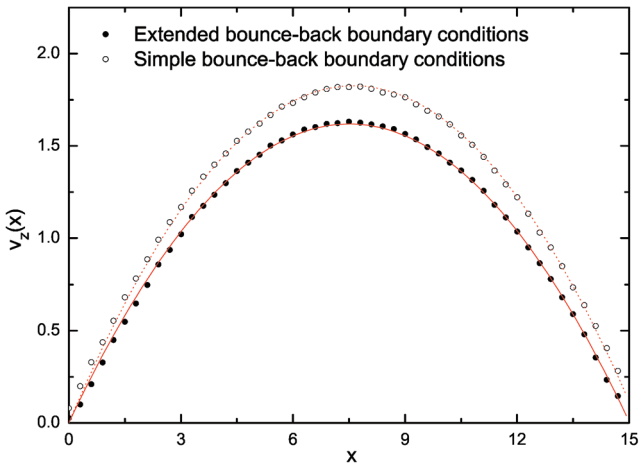


FIG. 4. Velocity-field profile in $z$-direction along the $x$-axis for a channel of volume $V=(15\times15\times25)$ and solvent density $\rho=5$. The open circles represent the results for simple bounce-back boundary conditions, while the full circles show the modified boundary conditions; see the text and Eq. (23).

particles along the channel length can be noticed; hence, these perturbations lead to a severe decrease of usable space in the simulation box.

The use of gravitationally driven flow, which is adopted in this contribution, does not distort the velocity-field and density profiles, and hence no artificial tricks are needed to suppress the inhomogeneities. The external force is given by $\mathbf{F}=\rho\mathbf{g}$, where $\mathbf{g}=g\hat{\mathbf{z}}$, and can easily be incorporated into the streaming step as follows:

$$\mathbf{r}_i'(t+\Delta t)=\mathbf{r}_i'(t)+\Delta t\mathbf{v}_i'(t)+\frac{\Delta t^2}{2}g\hat{\mathbf{z}}, \tag{21}$$

$$\mathbf{v}_i'(t+\Delta t)=\mathbf{v}_i'(t)+\Delta t g\hat{\mathbf{z}}, \tag{22}$$

with $\hat{\boldsymbol{z}}$ denoting the unit vector in flow direction. Furthermore, the strength of the gravitational field can be varied by tuning the acceleration constant $g$, and a steady Poiseuille flow builds up self-consistently after a short time. Periodic boundary conditions are applied for the walls in the $y$- and $z$-directions and no-slip boundary conditions in the $x$-direction. For planar walls coinciding with the boundaries, such conditions are conveniently simulated by employing a bounce-back rule, i.e., the velocities of particles that hit the walls are inverted after the collision. However, the walls will generally not coincide with or even be parallel to the cell boundaries. Furthermore, partially occupied cells can also emerge from the cell-shifting, which is unavoidable for small mean free paths $\lambda$. Lamura *et al.*[30] have demonstrated that the bounce-back rule has to be modified in such a case. Indeed, as can be seen in Fig. 4, the velocity profile arising from simple bounce-back conditions does not extrapolate to zero at the walls. One possible solution is to refill all those cells that are cut by the walls and therefore have a number of particles $n_j$ smaller than the average number $n_{\mathrm{avg}}$ of the bulk cells. The velocities of these virtual particles are then drawn from a Maxwell–Boltzmann distribution of zero average velocity and the same temperature $T$ as the fluid. However, since the sum of random vectors drawn from a Gaussian distribution is again Gaussian-distributed, the individual velocities never have to be determined explicitly. Instead, the average velocity $\mathbf{u}_j$ of Eq. (20) can be modified as follows:

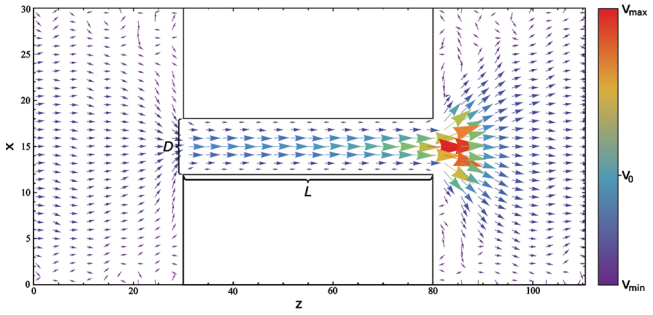


FIG. 5. Color-coded velocity-field profile in the flow-gradient plane in a system with $L=50.0$, $D=6.0$, and $g=0.05$. The length of the arrows is proportional to the local speed of the solvent particles.

$$\mathbf{u}_j=\frac{\Sigma_{i\in\mathcal{V}_j}\mathbf{v}_i'+\mathbf{v}_{\mathrm{G}}}{n_{\mathrm{avg}}}, \tag{23}$$

where the components of $\mathbf{v}_{\mathrm{G}}$ are normally distributed with variance $(n_{\mathrm{avg}}-n_j)k_BT$ and zero average. The so-obtained velocity profile is shown in Fig. 4 along with a parabolic curve fit and shows very good agreement between the theoretical predictions and the simulation results. This approach can be easily applied in order to properly incorporate narrowings into the system. In Fig. 5, we show the color-coded velocity-field in the flow-gradient plane, where the no-slip boundary conditions along the channel walls as well as the parabolic shape of the profile in the center of the channel are clearly visible.

Furthermore, thermostatting has been applied, as it is necessary in any nonequilibrium simulation, to avoid viscous heating. The thermostat employed was based on rescaling the random part of the velocities to maintain constant $T$ and has been described in Ref. 24. The MPCD parameters employed were $\alpha=130$, $\lambda=0.1$, and $\rho=5$. An important quantity of the solvent that can, among others, be calculated in this model[24,26] is the dynamical viscosity $\eta$. In our simulations, its numerical value reads $\eta=3.955\sqrt{\epsilon m}/\sigma^2(\approx1/3$ mPa s).

Coupling of the solvent dynamics with the dissolved dendrimer is achieved by including any monomer that happens to be in a cell (due to the choice for the cell size, there is *at most* one monomer there) in the collision step [Eq. (20)]. In this way, the nonrandom part of the monomer velocity is equal to that of the center of mass in the corresponding cell, and the molecule gets transported along the local flow. This coupling is part of the MPCD-scheme. On top of this, usual MD is performed with the intermolecular forces arising from the potentials of Eqs. (14) and (15) between the monomers, completing the hybrid simulation scheme. For the usual MD-step, we use a Verlet algorithm with $\Delta t_{\mathrm{MD}}=0.001\sigma\sqrt{m/\epsilon}$. At the beginning of the simulation, the polymer's center of mass was pinned directly ahead of the channel entrance, at a distance of $5.0\sigma$. After an equilibration period of $2\times10^5$ MD steps, the polymer was released from its pinning position and allowed to flow with the streaming solvent.

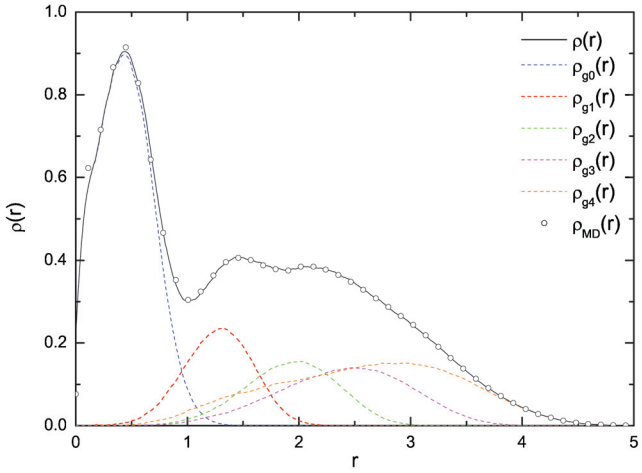


FIG. 6. The generation-resolved monomer density distribution $\rho(r)$ of a trifunctional $G4$-dendrimer. For the overall density profile, we show both the result from the MPCD (solid line) and that from a conventional MD without solvent (points).

A necessary prerequisite for any nonequilibrium simulation method is that it should reproduce the equilibrium results when the external driving fields (in our case, Poiseuille flow) are switched off. Therefore, as a preliminary check, we have performed MPCD simulations with explicit solvent and dendrimers in equilibrium and calculated generation-resolved density profiles, comparing them with those arising from standard, equilibrium MD employing the same dendrimer model. Figure 6 shows a typical density distribution, and an excellent agreement between the results can be observed, confirming the soundness of the approach.

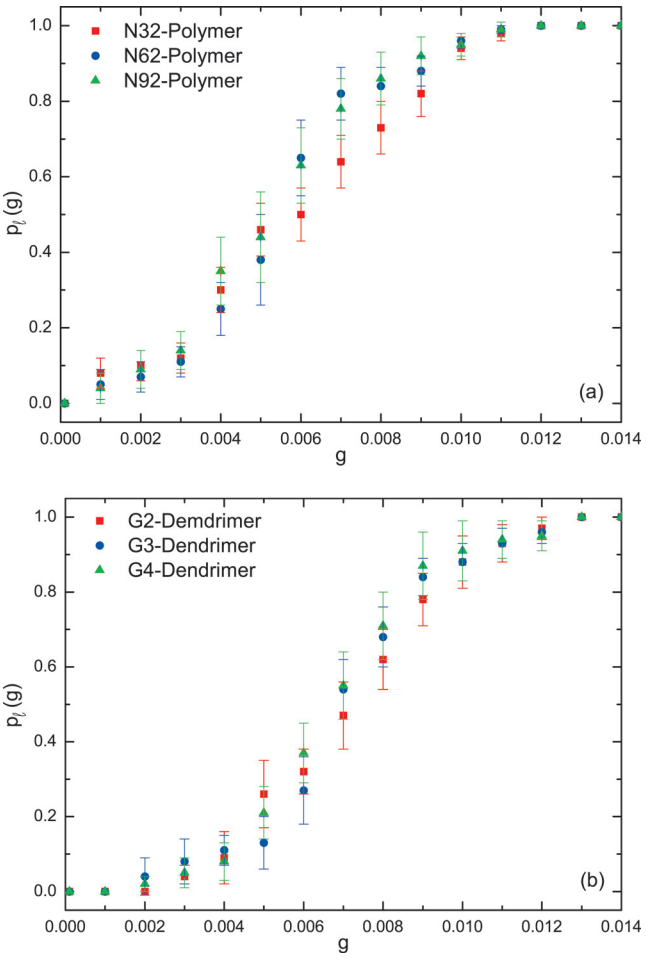


FIG. 7. Translocation probability $p$ through a slit of width $D=2.0$ for polymer chains of different lengths (a) and dendrimers of different generation numbers (b).

## IV. RESULTS

We begin with the question regarding the critical current $J_c$, with the purpose of checking the main finding of the theoretical approach (Sec. II), stating that $J_c$ is independent of the molecular weight. For this purpose, we have conducted a series of simulations for a given total time and counted the fraction of instances for which the molecules went through. In Fig. 7 we plot the translocation probability $p_\ell(g)$ through a slit of width $D=2.0$, as a function of the gravitational force $g$, for linear polymers and dendrimers of various sizes. For each parameter set, we have performed 50 simulations of $\ell=10^7$ time steps. The results in Fig. 7(a) pertain to linear polymers and provide an independent confirmation of similar findings by Markesteijn *et al.*,[16] obtained by means of Lattice–Boltzmann techniques, whereas results in Fig. 7(b) refer to dendrimers. We see a smooth transition from $p_\ell(g)=0$ to $p_\ell(g)=1$ as $g$ increases. At this point, we would like to emphasize that the continuous nature of $p_\ell(g)$ is only due to the finite number of time steps in our simulation. Furthermore, we see that in both cases the probability is completely independent of $N$, which is in full agreement with previous results[14,16] as well as our own theoretical prediction. When the results for linear polymers and dendrimers are compared, it is visible that the threshold flux is slightly higher for dendrimers, which is due to their more compact structure. Furthermore, we suspect that $J_c$ would become larger if the dendrimer's degrees of freedom were constricted by internal bond and torsion angles. However, once the molecule is sucked into the channel, the increased rigidity of the polymer should accelerate its motion through the channel, thereby shortening the translocation times.

We now generalize the discussion to consider channel widths $D$ that are both smaller and slightly larger than the dendrimer size. Once the macromolecule has entered the channel, the main quantity of interest is the translocation time $\tau$. In Fig. 8, we show $\tau$ as a function of the channel width $D$ for both linear and regularly branched polymers; the simulation has been performed for $g=0.05$ and averaged over 50 runs. When the translocation time of the whole molecule is considered, i.e., the time span between the entry of the first bead and the exit of the last bead, dendrimers have a slightly smaller passage time. This is again due to their rather compact structure, whereas linear polymers get elongated rather easily in the flow direction, and hence more time is needed until all monomers have passed through the narrowing. However, these differences vanish completely when the center of mass is considered instead of the whole polymer.

To better analyze the differences between linear polymers and dendritic structures, it is useful to have a look at their individual flow behavior through the narrowing. In Fig. 9, we show the position of the polymer's center of mass in

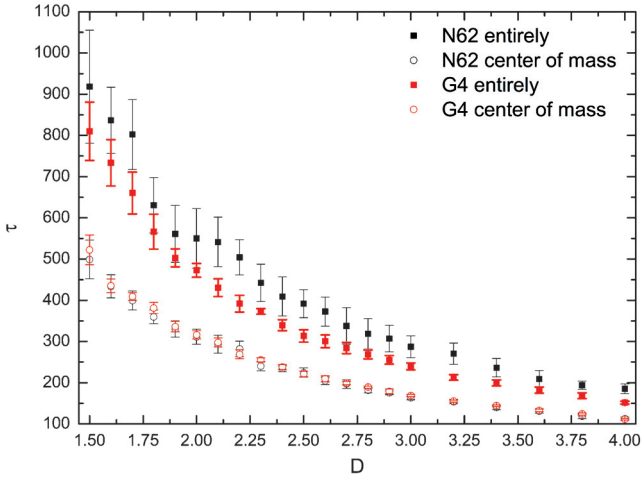


FIG. 8. Translocation time $\tau$ of a linear polymer and a G4-dendrimer with each $N=62$ beads as a function of the channel width $D$. The simulation has been carried out at $g=0.05$ for a channel of length $L=30.0$.

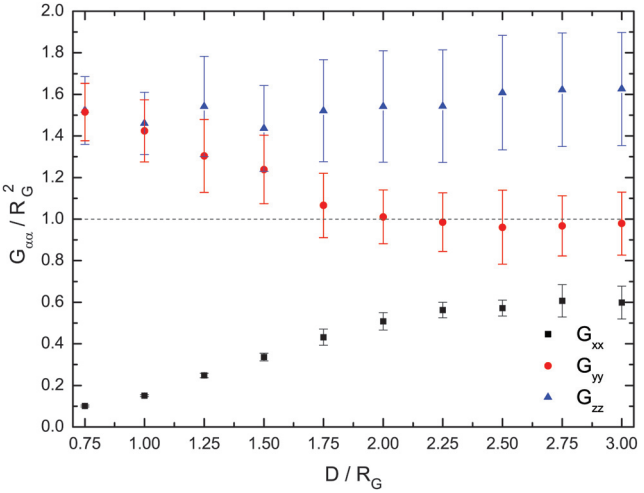


FIG. 10. Diagonal components $G_{\alpha\alpha}$ of the average gyration tensor as a function of the channel width $D$ for a G4-dendrimer with $N=62$ beads. The simulation has been carried out at $g=0.05$ for a channel of length $L=80.0$.

flow direction $z$ as a function of time $t$ for channels of length $L=30$ and various widths $D$. Since we are mainly interested in the impact of the confinement, we only plot the regime between channel start ($z=40$) and channel end ($z=70$). The simulations have been performed for $g=0.05$, and each curve has been averaged over 25 measurements. Here, it is well-visible that though the translocation times $\tau$ of linear and regularly branched polymers are almost identical, their detailed flow behavior is nevertheless quite different. Dendritic structures exhibit a much broader regime of ballistic propagation (translocation with constant speed) than chain polymers with the same monomer number $N$. The reason for this behavior is that, although the linear polymer's center of mass has already entered the channel, a significant part of the polymer is still outside the capillary and needs to be sucked in. This leads to an overall hindrance, which manifests itself in the lack of linear part in the curves $t(z)$ for linear chains.

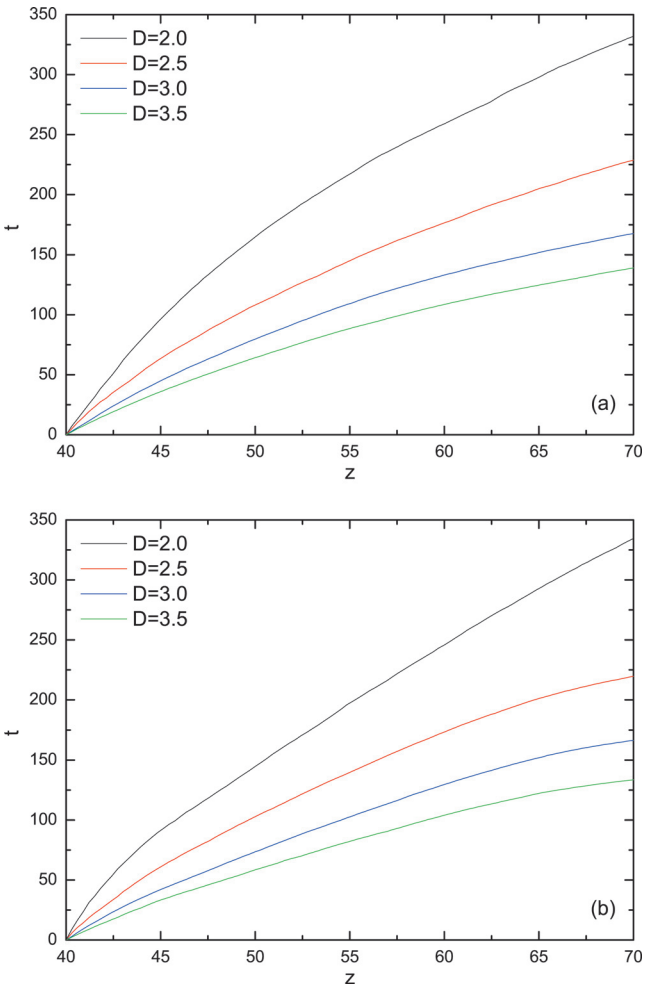


FIG. 9. The $z$-position of the center of mass inside a channel of length $L=30.0$ at $g=0.05$ for a polymer chain with 62 beads (a) and a dendrimer of fourth generation (b).

Turning our attention to the molecular deformations inside the channel, we have measured the diagonal components $G_{\alpha\alpha}$ of the average gyration tensor, Eq. (18), as a function of the channel width $D$. In this way, we can quantify the impact of the constriction on the polymer shape. Results of the simulation, which referring to conditions $g=0.05$ and channel length $L=80.0$, are shown in Fig. 10. Surprisingly, even for large channel widths, $D>2R_G$, neither $G_{zz}$ nor $G_{xx}$ approach the equilibrium (bulk) radius of gyration ($R_g=2.78\pm0.04$). Instead, the dendrimer becomes elongated along the $z$-axis by a factor of approximately 1.5 and subsequently shrinks in $x$-direction by about the same factor. This deformation is due to the two-dimensional parabolic flow profile of the solvent, and as a first approximation, the solvent flow can be considered as a superposition of two opposite shear flows, which act on the polymer. In such systems, deformation has been observed both for dendrimers[24] and other soft macromolecules.[32,33] For linear polymers, such an analysis is less interesting since they get elongated rather easily along the flow direction and almost reach their maximum extension.

Consistent with the above discussion, we have observed in our simulations that the polymer swims equidistant to both channel walls, where it is also exposed to the strongest fluid current. This centering is due to the hydrodynamic interactions mediated by the solvent and has been already observed

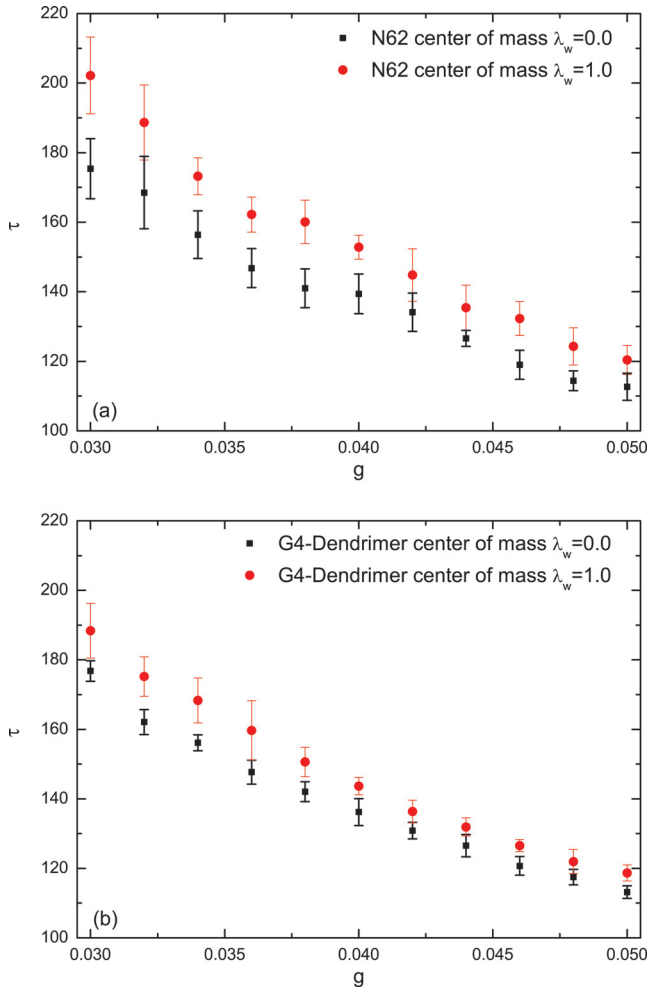


FIG. 11. Translocation time of a linear polymer (a) and a G4-dendrimer (b) with each $N=62$ beads as a function of $g$. The simulation has been carried out for a channel of width $D=4.0$ and length $L=30.0$.

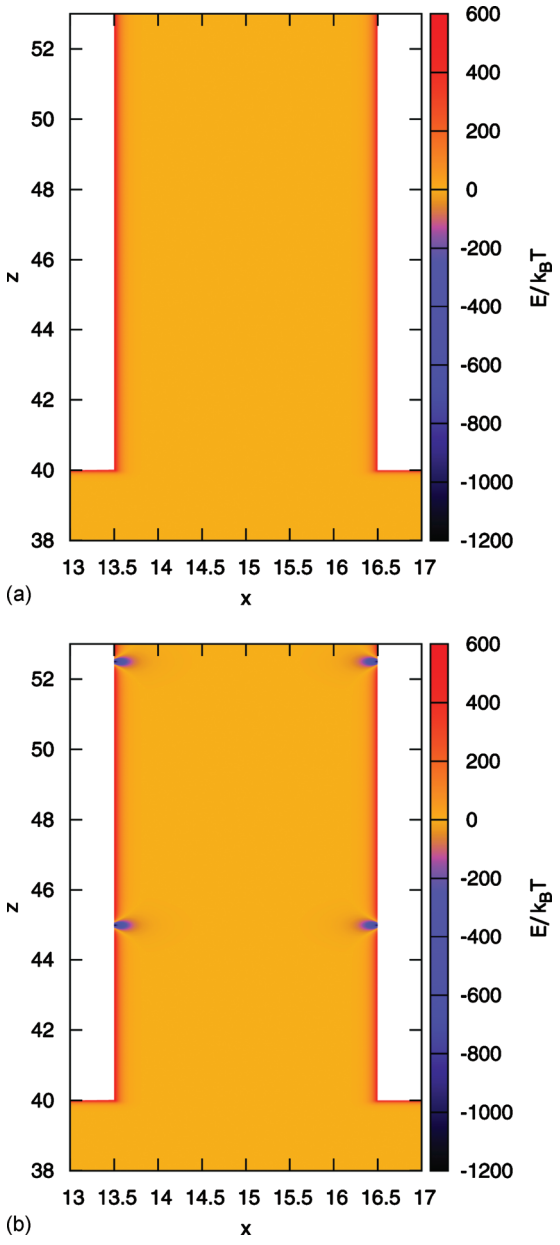


FIG. 12. Color-coded potential landscape in the flow-gradient plane close by the channel entrance. Purely repulsive walls (a) and repulsive walls covered with highly attractive patches (b). The extension of the line shaped patches is along the $y$-axis.

in previous simulations.[34] By adding an attractive part to the wall potential, i.e., turning into the case $\lambda_w=1.0$, one could expect that it is possible to "push" the polymers toward the channel walls and thereby slow down their motion (translocation) inside the channel since the fluid velocity is much smaller in the vicinity of the channel walls. In Fig. 11, we show the translocation time $\tau$ of a polymer chain in the case of purely repulsive and partly attractive walls. Although a small retardation is measurable, the impact is far from being significant in the case of linear polymers and almost nonexistent for dendrimers. Details of the wall-monomer interactions seem to be immaterial, at least as long as the walls are smooth.

Real walls on the other hand are rarely smooth, and at the nanoscale, atomic details become relevant. Of particular interest in this work is the possibility to decorate the walls with attractive patches. This can be achieved either with chemical patterning on the walls or, more importantly, through insertions of suitable entities, such as peptides intruding rigid bilayer membranes, as demonstrated in the recent work of Smith *et al.*[35] Accordingly, instead of a homogeneous attraction, we cover the channel walls with $N_p$ linelike, highly attractive patches. In Fig. 12, we show the color-coded potential landscape both in the simple, purely repulsive case and in the case of repulsive walls covered with the line shaped patches. The patches could model "docking sites" at which a dendrimer should temporarily reside, with the purpose of delivering an encapsulated cargo at the appropriate place, whereas the solvent (blood) flow should carry away the remaining molecule at longer times.

Due to the noncontinuous shape of the potential, its gradient leads to a nonzero contribution in the flow direction, which results in a severe sticking of the polymers. This is especially evident in the case of linear polymers, where the polymer almost completely aligns against one channel wall and thus only experiences a very weak solvent flow [see Fig. 13(a)]. Dendrimers on the other hand cannot flatten entirely against one channel wall; instead, the extremities gravitate toward the patches, while the core of the polymer remains in

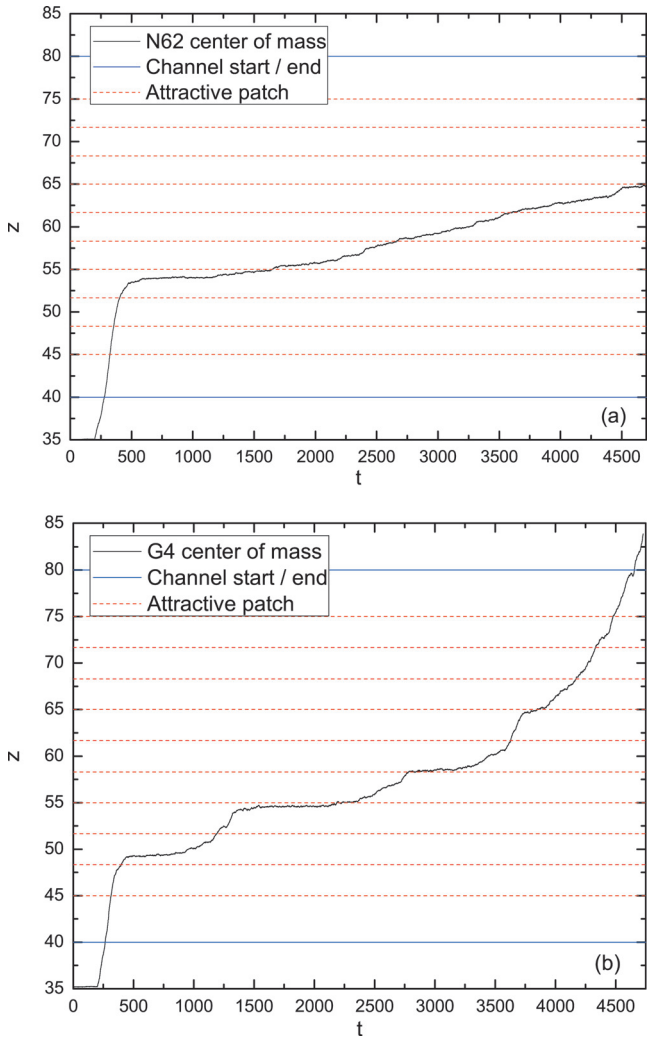


FIG. 13. Spatiotemporal evolution of a linear polymer's (a) and a G4-dendrimer's (b) center of mass in a channel with $L=40.0$ and $D=6.0$ with $N_p=10$ attractive patches at $g=0.015$.

the channel center. Eventually one arm detaches from its patch, hence releasing the whole polymer. Then, the whole macromolecule moves a bit further inside the channel until it approaches the next patch and the whole process repeats itself. This procedure is well-visible on the basis of the plateaus in Fig. 13(b), where the position of the dendrimer's center of mass is plotted against the time. These findings are remarkable since now, in contrast to the case of homogeneously attractive walls, the retardation is highly dependent on the shape of the polymers. Hence, such a setup can be used to separate dilute linear/dendritic polymer mixtures. We also note that, although the results presented here pertain to both walls being decorated with the same patches that face each other, they remain essentially unchanged also in the case of a single patterned wall.

Finally, to quantify this retardation effect more thoroughly, we measured the translocation time $\tau_p$ in the presence of patches for two channels of different widths ($D=4.0<2R_G$ and $D=6.0>2R_G$) and derived the slowdown compared to the case of purely repulsive walls. The results are plotted as a function of $N_p$ and are shown in Fig. 14. A quite remarkable slowdown is evident in both cases, where

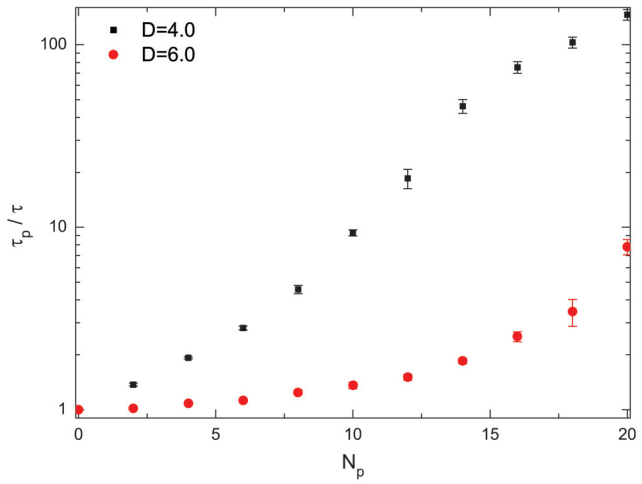


FIG. 14. Slowdown factor of a G4-dendrimer in a channel of length $L=40.0$ at $g=0.05$, plotted against the number of attractive patches $N_p$.

in the narrower channel, a slowdown by two orders of magnitude can be achieved for the case of $N_p=20$ patches. The relevance of the channel width $D$ is due to the rather short-ranged nature of the patch potential; therefore, the broader the channel, the less important the presence of patches on the channel walls. Concerning the interpatch spacing, we have shown that the impact of the sticky patches vanishes for the both extreme cases $L/N_p \to 0$ (smooth walls) and $L/N_p \to \infty$ (no patches). We therefore expect that the translocation time is maximal when the interpatch spacing is of the order of the dendrimer size since this configuration allows the dendrimer to dock on one patch, while at the same time, a few monomer can dock on neighboring patches. Three videos showing the progression of linear and dendritic polymers through patchy channels, compared with a dendrimer flowing in a smooth channel, are provided as supplementary material in the online version of this paper.[36]

## V. CONCLUSIONS

We have employed a theoretical scaling analysis to establish the independence of the current injection threshold into narrow channels for low-generation dendrimers, which has been confirmed by hybrid computer simulations. The latter allows for an efficient coupling between hydrodynamic effects and polymer dynamics and offer an excellent computational tool to study the transport of polymers through narrow channels. We have established that the translocation times of dendrimers and linear polymers of the same molecular weight along such channels are quite similar to one another as long as the channel walls are smooth. However, wall granularity has dramatic effects both on the translocation times as such and on the relative duration of transport between dendrimers and polymers. In particular, localized attractive linear patches bring forward for the dendrimers a kind of motion akin to "walking along the wall," with long plateaus of residence times on the attractive patches, whereas linear polymers do not escape the patchy channel within simulation times.

Our findings establish that dendritic molecules are peculiar in their transport properties along narrow channels, and

they express, also under flow, their unusual character as hybrids between compact colloids and flexible polymeric objects, already known from their equilibrium behavior.[18,20,21] The long residence times of the dendrimers on the wall traps open up the interesting possibility that when the former are loaded with some chemical cargo (e.g., a drug molecule), the latter could be delivered on the patch and be absorbed there during the carrier's residence time, while the blood flow "washes away" the empty dendrimer afterward. This topic, along with investigations on the effects of more complex channel geometries and charge, will be the subject of future investigations.

## ACKNOWLEDGMENTS

A.N. acknowledges the Studienstiftung des Deutschen Volkes for financial support. This work has also received partial support by the SFB-TR6, Project C3.

[1] A. Milchev, K. Binder, and A. Bhattacharya, J. Chem. Phys. **121**, 6042 (2004).
[2] W. Sung and P. J. Park, Phys. Rev. Lett. **77**, 783 (1996).
[3] M. Muthukumar, J. Chem. Phys. **111**, 10371 (1999).
[4] M. Muthukumar, Phys. Rev. Lett. **86**, 3188 (2001).
[5] M. Muthukumar, J. Chem. Phys. **118**, 5174 (2003).
[6] P. J. Park and W. Sung, J. Chem. Phys. **108**, 3013 (1998).
[7] E. A. Di Marzio and A. J. Mandell, J. Chem. Phys. **107**, 5510 (1997).
[8] J. Chuang, Y. Kantor, and M. Kardar, Phys. Rev. E **65**, 011802 (2001).
[9] J. K. Wolterink, G. T. Barkema, and D. Panja, Phys. Rev. Lett. **96**, 208301 (2006).
[10] S. K. Sia and G. M. Whitesides, Electrophoresis **24**, 3563 (2003).
[11] D. Branton, D. W. Deamer, A. Marziali, H. Bayley, S. A. Benner, T. Butler, M. Di Ventra, S. Garaj, A. Hibbs, X. Huang, S. B. Jovanovich, P. S. Krstic, S. Lindsay, X. S. Ling, C. H. Mastrangelo, A. Meller, J. S. Oliver, Y. V. Pershin, J. M. Ramsey, R. Riehn, G. V. Soni, V. Tabard-Cossa, M. Wanunu, M. Wiggin, and J. A. Schloss, Nat. Biotechnol. **26**, 1146 (2008).
[12] M. Zwolak and M. Di Ventra, Rev. Mod. Phys. **80**, 141 (2008).
[13] J. J. Kasianowicz, E. Brandin, D. Branton, and D. W. Deamer, Proc. Natl. Acad. Sci. U.S.A. **93**, 13770 (1996).
[14] T. Sakaue, E. Raphaël, P.-G. de Gennes, and F. Brochard-Wyart, Europhys. Lett. **72**, 83 (2005).
[15] P. G. de Gennes, Adv. Polym. Sci. **138**, 92 (1999).
[16] A. P. Markesteijn, O. B. Usta, I. Ali, A. C. Balazs, and J. M. Yeomans, Soft Matter **5**, 4575 (2009).
[17] P. G. de Gennes, *Scaling Concepts in Polymer Physics* (Cornell University Press, Ithaca, 1979).
[18] I. O. Götze and C. N. Likos, Macromolecules **36**, 8189 (2003).
[19] C. N. Likos, S. Rosenfeldt, N. Dingenouts, M. Ballauff, P. Lindner, N. Werner, and F. Vögtle, J. Chem. Phys. **117**, 1869 (2002).
[20] H. M. Harreis, C. N. Likos, and M. Ballauff, J. Chem. Phys. **118**, 1979 (2003).
[21] M. Ballauff and C. N. Likos, Angew. Chem., Int. Ed. **43**, 2998 (2004).
[22] C. Gay, P. G. de Gennes, E. Raphael, and F. Brochard-Wyart, Macromolecules **29**, 8379 (1996).
[23] G. S. Grest, K. Kremer, and T. A. Witten, Macromolecules **20**, 1376 (1987).
[24] A. Nikoubashman and C. N. Likos, Macromolecules **43**, 1610 (2010).
[25] C. N. Likos, Phys. Rep. **348**, 267 (2001).
[26] A. Malevanets and R. Kapral, J. Chem. Phys. **110**, 8605 (1999).
[27] G. Gompper, T. Ihle, D. M. Kroll, and R. G. Winkler, Adv. Polym. Sci. **221**, 1 (2009).
[28] T. Ihle and D. M. Kroll, Phys. Rev. E **63**, 020201 (2001).
[29] A. Malevanets and R. Kapral, J. Chem. Phys. **112**, 7260 (2000).
[30] A. Lamura, G. Gompper, T. Ihle, and D. M. Kroll, Europhys. Lett. **56**, 319 (2001).
[31] E. Allahyarov and G. Gompper, Phys. Rev. E **66**, 036702 (2002).
[32] M. Ripoll, R. G. Winkler, and G. Gompper, Phys. Rev. Lett. **96**, 188302 (2006).
[33] M. Kraus, W. Wintz, U. Seifert, and R. Lipowsky, Phys. Rev. Lett. **77**, 3685 (1996).
[34] Y.-L. Chen, H. Ma, M. D. Graham, and J. J. de Pablo, Macromolecules **40**, 5978 (2007).
[35] M. B. Smith, D. J. McGillivray, J. Genzer, M. Lösche, and P. K. Kilpatrick, Soft Matter **6**, 862 (2010).
[36] See supplementary material at http://dx.doi.org/10.1063/1.3466918 for videos of a dendrimer flowing in a smooth and a patchy slit as well as a linear polymer progressing in a patchy slit.